Research Article

BIOMEDICAL Journal of Scientific & Technical Research

ISSN: 2574 -1241

DOI: 10.26717/BJSTR.2021.37.005934

Evaluation of the Antitumor Activity of Newly Synthesized Cisplatin/Mgo/Chitosan Nanocomposite in The Treatment of Lung Carcinoma Induced in Rats

Aya Sh R Shaaban[1], Ahmed MH Salem[1], Faten I Abou Albada[2]*, Marwa GA Hegazy[1], Fatma SM Moawed[3] and Ekrami A Hassan[1]

[1]*Department of Biochemistry, Faculty of science, Ain Shams University, Egypt*

[2]*Polymer Chemistry Department, National Center for Radiation Research and Technology, Atomic Energy Authority, Egypt*

[3]*Health radiation research, National Center for Radiation Research and Technology, Atomic Energy Authority, Egypt*

***Corresponding author:** Faten I Abou Albada, Polymer Chemistry Department, National Center for Radiation Research and Technology, Atomic Energy Authority, Cairo, Egypt

ARTICLE INFO

Received: June 16, 2021

Published: July 06, 2021

Citation: Aya Sh R Shaaban, Ahmed MH Salem, Faten I Abou Albada, Marwa GA Hegazy, Fatma SM Moawed, Ekrami A Hassan. Evaluation of the Antitumor Activity of Newly Synthesized Cisplatin/Mgo/Chitosan Nanocomposite in The Treatment of Lung Carcinoma Induced in Rats. Biomed J Sci & Tech Res 37(1)-2021. BJSTR. MS.ID.005934.

Abbreviations: SCLC: Small Cell Lung Carcinoma; LC: Lung Cancer; NSCLC: Non-Small Cell Lung Carcinoma; DMEM: Dulbecco's Modified Eagle Medium; ATCC: American Type Culture Collection; GAPDH: Glyceraldehyde 3-Phosphate Dehydrogenase; PTEN: Phosphatase and Tensin Homolog

ABSTACT

The present study aimed to evaluate whether using chitosan encapsulated cisplatin nanocomposite (MgO/CS/Cis) improved the antitumor efficiency than that in case of using free Cisplatin (Cis) for targeted Lung Cancer (LC) both *in vitro* and *in vivo* or not Methods. Our results revealed that Cis or MgO/CS/Cis treatment could suppress the propagation in A-549 cancer line. Further, notable declines in the expression levels of proteins regulatory PI3K/ PTEN/ AKT/mTOR, with overexpression of the proteins regulating MAPK-38 pathway following the administration of either Cis or MgO/CS/Cis. The high caspase-9 and inhibition expression of KRAS associated reduced Bcl2 levels were shown to have marked pro-apoptotic effects of Cis or MgO/CS/Cis. Results also, showed that the newly synthesized cisplatin nanocomposite can perform the same role of cisplatin in treating lung cancer while minimizing the usual side effects caused by using cisplatin alone. Histopathological screening confirmed these outcomes. The newly synthesized MgO/CS/Cis therapy has also shown substantial improvements in the efficacy of Cis anti-cancer and reduced the amount of normal cisplatin-treated side effects. These results suggest that MgO/CS/Cis encapsulated nanocomposite can function as a power control for accurate cancer treatment beyond cisplatin drugs which should attract further studies.

Keywords: Lung Cancer; Cisplatin; MgO/CS/Cis Encapsulated

Introduction

Lung cancer is the leading cause of cancer death among men and the second leading cause of cancer death among women worldwide. In Egypt it is one of the collective sites of cancer especially in males [1]. The main types of lung cancers are Small Cell Lung Carcinoma (SCLC), also called oat cell cancer, and Non-Small Cell Lung Carcinoma (NSCLC). Tobacco smoking in addition to certain occupational exposures and air pollution are the main causes for lung carcinoma. The most common indicators are coughing, weight loss and shortness of breath [2]. Lung cancer may be recognized on ribcage radiograph and calculated tomography (CT scan). The diagnosis is established with a biopsy. This is usually achieved by bronchoscopy or CT-guided biopsy. Conduct and projection can

be reliant on the histological type of cancer, the stage (degree of spread), and the patient's worldwide well-being, measured by performance prominence [3]. Ordinary actions include surgery, chemotherapy, and radiotherapy. NSCLC is sometimes well-handled with surgery, whereas SCLC usually responds well to chemotherapy and radiation therapy. This is comparatively because SCLC often punctures relatively early, and these handlings are usually better at getting to cancer cells that have feast to other portions of the body.

There is a moderately little certain progress in lung cancer therapy, even with the current progress in cancer therapy, the surgery, radiation and chemotherapy remain the main treatment strategies in lung cancer management [4]. Once cisplatin introduced, chemotherapy has become the highest confirmed treatment approach in lung cancer treatment. Lately, in spite of applying numerous new drugs with improved potency to lung cancer, cisplatin remains the main drug for lung cancer treatment [5]. Cisplatin was unintentionally discovered by Barnett Rosenberg in 1965 and documented as an anticancer drug since then. It was employed for the treatment of a wide array of solid malignancies, including lung cancers [6]. Cisplatin employs anticancer effects through the generation of DNA lesions followed by the activation of the DNA damage response and the induction of mitochondrial apoptosis [5]. Despite of good clinical success of cisplatin, it lacks tumor tissue selectivity which resulted in some severe side effects [7]. Improvements in nanotechnology with the growing needs in biomedical applications have driven the development of multifunctional nanoparticles [8].

Nanotechnology as a new field of research became effectively applied to human health because it offers novel approaches for treating many human diseases, including cancer [9]. Most nanomaterials display special characteristics which make them useful for a wide variety of biotechnologies. These properties were used to build powerful tools for therapy and/or diagnosis [10]. Nanomaterials can be used as cytotoxics, and/or enhancers of standard chemotherapies, as well as, drug delivery systems, where they can provide great help in reducing the side effects of conventional drugs [11]. The aim of the present study was to estimate whether Cisplatin encapsulated by biocompatible chitosan nanocomposites modified with magnesium oxide nanoparticles can improve the anti-tumor effect of Cisplatin *in vitro* and *in vivo.*

Materials and Methods

Chemicals

Chitosan with average molecular weight (300,000) was purchased from Sigma Co. USA. Magnesium nitrate hexahydrate ($MgNO_3.6H_2O$), NaOH and all other reagents were of analytical grade, and they were used without further purification, and purchased from Acmatic Co. Egypt. Urethane was purchased from Sigma-Aldrich Corporation (USA). Cisplatin (cis-PtCl2 $(NH_3)_2$) was obtained from Oncotec Pharma Produktion GmbH as solution for infusion in a vial of 10 mL Cisplatin Mylan (1mg/mL).

Nanoparticles Synthesis

Preparation of MgO Nanoparticles Encapsulated with Chitosan: First, 1% chitosan solution was prepared by dissolving 1gm in 1% acetic acid solution (100ml) under vigorous stirring using magnetic stirrer over night until complete homogeneity. Second, 1M magnesium nitrate hexahydrate solution was prepared by dissolving appropriate amount in 100ml distilled water with stirring. Equal amounts of chitosan and magnesium nitrate solutions were mixed in a beaker (250ml) very well by stirring for one hour, to the resulted mixture, 40ml of NaOH solution (1M) was added drop wisely and very slowly until a milky white suspension is formed. The milky white suspension is washed with distilled water by decantation several time to remove excess NaOH then completed to 100ml with distilled water. 20ml of Cisplatin was added to the previous mixture and stirring is continued for another one hour. The MgO/CS/Cis milky white dispersion then exposed to gamma radiation to degrade chitosan molecular chains to very low molecular weight and to ensure chitosan coating of Cisplatin and MgO. The highly suspended MgO/CS/Cis mixture was put in clean carefully sealed bottle until use.

Characterizations of MgO/CS and MgO/CS/Cis Nanoparticles

a) IR-Spectroscopy

The ATR-FTIR spectra of MgO/CS and MgO/CS/Cis nanoparticles were recorded using Fourier-Transform Infrared Spectroscopy FTIR-Vertex 70 spectrophotometer (Bruker, Germany).

b) Electron Scanning Microscopy (SEM)

Scanning electron microscopy of MgO/CS solid powder was obtained with JEOL JSM-5400 scanning electron microscopy (Japan), available at NCRRT.

c) Transmission Electron Microscopy (TEM)

TEM was used to observe the size and morphology of the formed MgO/CS nanoparticles. The suspension of MgO/CS in water was deposited on an ultrathin carbon supported Cu grid, and air-dried. TEM JEOL: JEM-100cx was used for this purpose.

d) X-ray Diffraction (XRD)

X-ray diffraction (XRD) data for MgO nanoparticles were collected using Rigaku 2550D/max VB/PC X-ray diffractometer supported with Cu Kα radiation (λ = 1.54056Å).

Cell Culture Study

Human lung cancer cell line (A-549) was obtained from the tissue culture unit of the VACSERA, Giza, Egypt and supplied through the American Type Culture Collection (ATCC). Cell lines were cultured in Dulbecco's Modified Eagle Medium (DMEM),

supplemented with 10% FBS, 0.2% sodium bicarbonate, and antibiotic/ antimycotic solution (100x, 1ml/100 ml of medium). The cell line was preserved in 5% CO2 at 37°C in humidified atmosphere. Before the tests, cell viability was evaluated. Cells with viability higher than 95% and passage number ranged from 20 to 22 were utilized in this study.

***In Vitro* Studies: (Cytotoxicity Assay using Crystal Violet):** A-549 cells were obtained from the American Type Culture Collection (ATCC, Rockville, MD), were used to determine the cell's cytotoxic effect of each of the tested treatments according to [12,13] which were determined using the MTT (3-[4,5-dimethylthiazol-2-yl]-2.5-diphenyl tetrazolium bromide) kit (Trevigen Inc., Gaithersburg, MD, USA) according to the manufacturer's information. In brief, cells were seeded on 96-well plates in a range of 103-105 cells/well in the presence or absence of Cis (0.64μg/ml) or MgO/CS/Cis (5.75μg/ml) in an ultimate volume of 100 μL of medium and were allowed to fasten overnight. The MTT reagent is added (10 μL per well) and the plate is incubated for 24 h to permit the reduction of the soluble yellow MTT to the insoluble purple formazan dye. Detergent reagent is added to each well to solubilize the formazan dye prior to measurement of the absorbance of each sample at 550-600 nm using a microplate reader. Six wells were used for each group. Cell proliferation was calculated as the percentage of cell proliferation in respect to untreated cancer cell line [14].

Experimental Animals

Male Wistar rats (weighing 122-153g) were purchased from the Nile Pharmaceutical Co., Cairo, Egypt. They were housed at the animal house at the National Center for Radiation Research and Technology. Upon influx, the animals were allowed to regulate for one week before launching the experiment. The animals were reserved under standard laboratory atmospheres of light/dark cycle (12/12h), a temperature of 25 ± 2 °C and humidity of 60 ± 5%. The rats were housed in birdcages with free entree to food and drinking water. They were delivered with a nutritionally suitable standard laboratory (pellet) diet. The study was convoyed in agreement with international procedures for animal experiments and permitted by the Ethical Committee at the National Center for Radiation Research and Technology (NCRRT), Atomic Energy Authority, Cairo, Egypt.

***In Vivo* Studies: (Determination of LD50 using Experimental Animals):** In screening drugs, determination of LD50 is usually an initial step in the assessment and evaluation of the toxic characteristics of a substance. The LD50 of the studied compounds was determined as described by Akhila et al.

Experimental Design

Animals were endorsed one week for adaptation, then randomly distributed into 6 groups (12 rats each): Group 1 (Control): normal rats, Group 2 (MgO/CS/Cis): rats were injected with 10% of LD50 of (MgO/CS/Cis): (5.75 mg/kg b.w./day i.p) for four weeks. Group 3 (Cis): rats were injected intra-peritoneal with cisplatin (0.64 mg/kg) for four weeks. Group 4 (LC): Rats were injected with urethane (dissolved in 0.9% normal saline) to induce LC, in a dose of 1g/kg, once a week for three consecutive i.p. injections of urethane, within a gap of 48 h in a week. The growth of lung tumors was initiated over a period of 9-12 weeks according to Parashar, et al. [15], Group 5 (LC+ MgO/CS/Cis): Rats with induced lung cancer (as in group 4) treated intraperitoneally with Cisplatin nano composite (5.75 mg/kg b.w./day) for 4 weeks. Group 6 (LC+Cis): rats with induced lung cancer (as in group 4) treated with Cis (0.64 mg/kg, IP) for four weeks. Blood tasters were withdrawn from the heart of each rat, under sunny anesthesia by diethyl ether. Blood was endorsed to thicken and then was centrifuged at 3000 rpm for 15 min. Immediately after blood sampling, animals were forewent by cervical dislocation; one lung was rapidly removed, washed in ice-cold saline, plotted to dry and weighed for biochemical studies. The second lung was dissected and was set aside for histopathological examination.

Detection of Bcl-2 and KRAS Genes Expression in Lung by Quantitative Real-Time Polymerase Chain Reaction (QPCR):

Total RNA was remote using QIAGEN tissue withdrawal kit (QIAGEN, USA) according to instructions of manufacturer. Quantitative real-time polymerase chain response (qRT-PCR) magnification and examination were achieved using an Applied Biosystems with software version 3.1 (StepOne™, USA). The qRT-PCR assess with the primer groups was adjusted at the annealing temperature. All complementary DNAs (cDNAs) were in duplicate and included with previously prepared samples for B-cell lymphoma 2 (bcl-2), and Kirsten Rat Sarcoma virus (K-RAS) with Glyceraldehyde 3-Phosphate Dehydrogenase (GAPDH) as an internal control, and water is used as non-template regulator to confirm the nonexistence of DNA contamination in the reaction mix.

Western Immunoblotting Analysis of mTOR and PTEN Protein in Lung Tissue Homogenate

Lung tissue proteins were extracted using TRIzol chemical then protein concentration was measured according to Bradford [15]. 20μg of protein per lane were separated with 10% sodium dodecyl sulphate-polyacrylamide gel electrophoresis (SDS-PAGE) and transferred onto PVDA membranes. Membranes were nursed at room temperature for 2 hours with blocking solution (5% non-fat dried milk in 10 mM TrisCl, pH 7.5, 100 mM NaCl, and 0.1% Tween 20), then incubated overnight at 4°C with primary antibodies towards mechanistic target of rapamycin (mTOR) and Phosphatase and Tensin Homolog (PTEN) proteins with β-actin as control. After washing three times in 10 mM Tris-Cl, pH 7.5, 100 mM NaCl, and 0.1% Tween 20, membrane was incubated with the secondary monoclonal antibody conjugated to horseradish peroxidase at

room temperature for 2h, and then membranes were washed four times with the same washing buffer. Membrane was developed and visualized by chemiluminescence using Amersham detection kit according to the manufacturer's protocols, then exposed to X-ray film. Primary and secondary antibodies were purchased from Cell Signaling Technologies, USA. The quantitatively measured mTOR and PTEN protein were quantified using a laser densitometer (Biomed Instrument Inc., USA) scanning.

Determination of AKT, PI3K and CAS-9 Lung Proteins Levels by using ELISA

Rat protein kinase B (Akt) (Ser473) levels in the lung tissue quantified using the RayBio ELISA Kit (PEL-Akt-S473-T; Raybiotech). Rat Phosphotylinositol 3 Kinase (PI3K) and Rat Caspase-9 (Cas-9) levels in lung tissue were quantified by ELISA Kit (Cat.MBS9712116), (Cat.MBS264306) from My BioSource (San Diego, California, USA) according to the manufacturer's guidelines.

Histopathological Study

After surrendering the rats, lung flesh was rapidly divided and excised, washed in saline solution, and cut into suitable pieces which were fixed in neutral buffered formalin (10%) for 24h according to the method assumed by Drury and Wallington and inspected by light microscope for histopathological examination.

Statistical Analyses

The SPSS (version 20) was used in data evaluation. Data were examined with one-way analysis of modification (ANOVA) monitored by a post hoc test (LSD) for several comparisons. The data were articulated as mean ± standard error (SE). P values < 0.05 were considered statistically significant.

Results

Characterization of MgO/CS and MgO/Cis Coated with Chitosan

IR Spectrum of Cisplatin and MgO/Cis Coated with Chitosan: The typical FTIR spectrum for the chitosan (100%) (CS), MgO nanoparticles, Cisplatin (CIS) and MgO/CIS coated with chitosan illustrated in (Figure 1). The IR of MgO nano-dispersion illustrates a stretching vibration mode appeared in the range 588-631 cm^{-1} attributed to the Mg-O-Mg as a broad band. Two distinct bands are seen at the waves number of 968.8 cm^{-1} and 1636 cm^{-1} and are attributed to the bending vibration of absorbed water molecule and surface hydroxyl group (-OH), respectively. A broad vibration band is seen in the wavenumber 3289.4cm^{-1} due to O-H stretching vibration of absorbed water molecule and surface hydroxyl group [16]. This is due to the adsorptions of water molecule onto the MgO surface when it is exposed to atmosphere. From FT-IR analysis of CIS solution, the main adsorption bands appeared are stretching vibrations of OH group at 3327.2 cm^{-1} due to water molecules and stretching vibration in the range 581.9 cm^{-1} to 603.6 due to Pt-O-Pt linkage. IR spectra of chitosan-MgO nanocomposite as in Figure 1 showed that the main functional groups of chitosan clearly appeared at: 3360 cm^{-1} (broad band of hydrogen bonded OH- groups), 2972 cm^{-1} (CH bond; CH3 groups), 1777 cm^{-1} (amide carbonyl groups), 1425 cm^{-1} (bending vibration of CH_2 groups), and 1058 cm^{-1} (asym. vibration of C=O) (Figure 1).

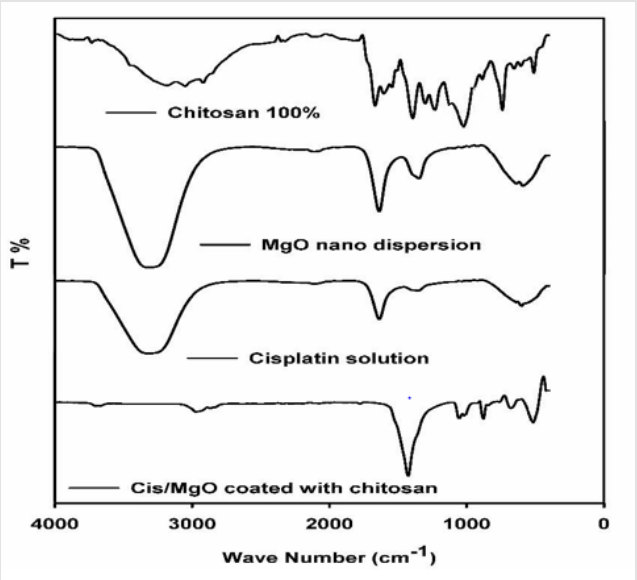

Figure 1: IR spectroscopy of Chitosan, MgO NPs, Cisplatin, and Cis/MgO coated with chitosan.

These bands are considered as signs for the conservation of the chitosan structure features even after the incorporation of the MgO nanoparticles inside the polymer matrix. Also, the absence of acetic acid bands in the spectrum indicated that the MgO/CS dispersion washed enough and neutralized completely upon sodium hydroxide treatment during preparation. Moreover, only small acceptable change in the bands of chitosan-MgO nanocomposite was credited to the impact of the combination of MgO nanoparticles. This shift in bands wave number was acquainted as consequence of chitosan reaction with metal oxides. The latter shifts are revealed, particularly at bands of NH and OH groups, which is proof for the H-bonding contact of these groups with MgO molecules.

X-Ray Diffraction Studies: The X-ray diffraction (XRD) pattern of prepared MgO nanoparticles is shown in (Figure 2) which proved that the synthesized Mg O is of hexagonal phase [17] which confirmed with the appearance of the characteristic peaks at 2Theta: 24.1o, 29.9o, 36.8o, 37.7o, 49.2o, and 55.9o. No impurities were detected in this pattern and all the crystal structures agreed with reported JCPDS data. The Average nanoparticle size was estimated using Scherer formulation:

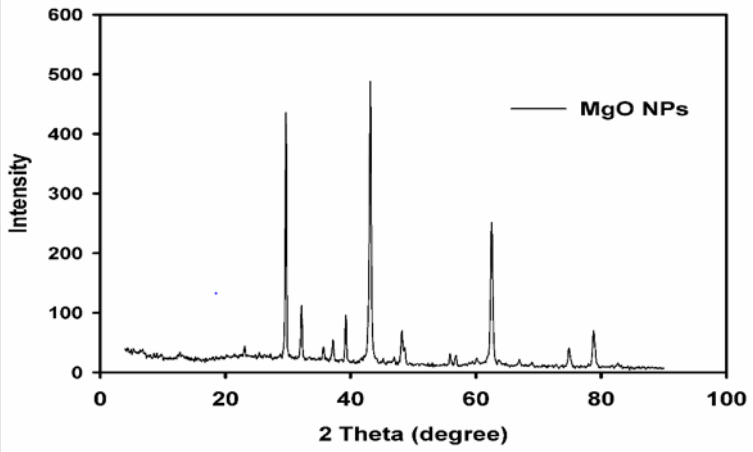

Figure 2: XRD pattern of pure MgONPs.

Crystallite average size $D = k\lambda / \beta(cos\ \theta)$

Where D is the crystallite size in nm, λ is the radiation wavelength (0.154 nm for Cu K), β is the bandwidth at half-height and θ is the diffraction peak angle and k is a constant (0.9). After a correction for the instrumental broadening, an average value of the Mg O nanoparticles size was found to be 4.26nm.

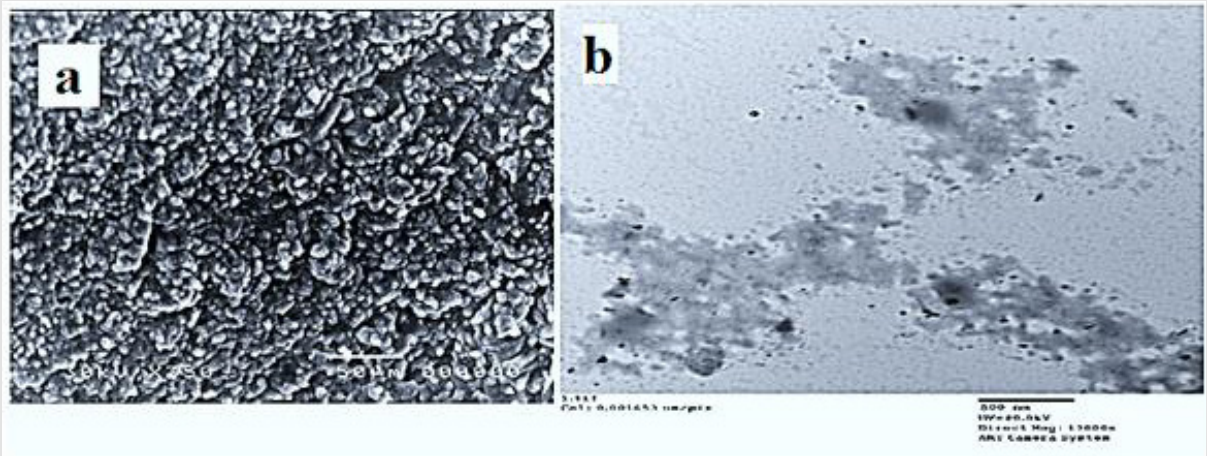

Figure 3:
a) SEM of MgO NPs (powder),
b) TEM photo of MgO NPs (dispersion).

Morphological Study of MgO: Scanning electron microscopy (SEM) and transmission electron microscopy (TEM) are the most applicable techniques used to figure out and analyze the morphology of materials, and to determine the size of particles in the nanoscale (TEM). By studying the Scanning electron microscopy (SEM) of pure MgO NPs (Figure 3a), it is found that the obtained MgO nanoparticles not only have highly compact crystalline structures without pores, but also their morphologies are exactly the same as those of corresponding Mg $(OH)_2$ precursors in the crystalline shape and sizes. TEM images of the MgO samples are shown also, in (Figure 3b). It can be seen from the TEM images of MgO nanoparticles (Figure 3b) that the particles appeared in an ordered structure of MgO nanoparticles with nearly the same size and shape. TEM photo of MgO nanoparticles illustrates that the MgO nanocrystallites have the same lamellar morphologies with hexagonal shape and the same sizes of nearly 10.32nm.

In Vitro Studies

The antitumor activity of MgO/CS/Cis and cisplatin was evaluated using A-549 cell lines. The chemical compounds were applied at various concentrations and results were presented in (Figure 4) showing that Cis IC50 = 7.53 µg/ml. while MgO/CS/Cis IC50 = 50.8 µg/ml.

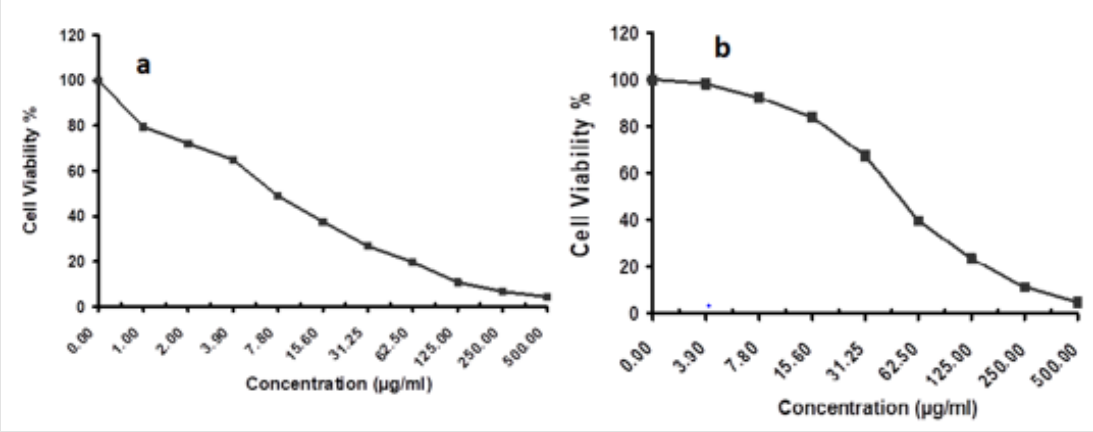

Figure 4: Cytotoxic activity of Cis and MgO/CS/Cis against A-549 cell line.

Effect of MgO/CS/Cis on Bcl-2 mRNA and KRAS mRNA Genes Expression Levels in Lung Tissue: The data summarized in (Tables 1 & 2) indicated that lung KRAS and Bcl2 were significantly increased in lung cancer rats' group when compared to control ones while there were a significant decrease in their levels when rats treated by either Cis or MgO/CS/Cis.

Table 1: Primer sequences of the studied genes.

Gene symbol	Primer sequence
Bcl-2	F: 5`-ATCGCTCTGTGGATGACTGAGTAC 3`
	R: 5`-AGAGACAGCCAGGAGAAATCAAAC 3`
KRAS	F: 5`-TGCTGAAAATGACTGAATATAAACTTGTG 3`
	R: 5`- GGTCCTGCACCAGTAATATGCA 3`
GAPDH	

Table 2: KRAS and Bcl2 genes expression levels in the different groups.

Group / Parameter	Control	Cis	MgO/CS/Cis	LC	LC+ Cis	LC+ MgO/CS/Cis
k-ras	$1.01^{b,c}$	$1.01^{b,c}$	$1^{b,c}$	$7.55\pm 0.04^{a,c}$	$2.5\pm 0.03^{a,b,c}$	$3.32\pm 0.05^{a,b}$
Bcl2	1 ± 0.01^{b}	1^{b}	0.99^{b}	$6.01\pm 0.27^{a,c}$	0.83 ± 0.02^{b}	1.01 ± 0.04^{b}

Note: Data expressed as mean ± standard error (mean ± SE), P value is significant at ≤ 0.05.

[a]significance vs control group

[b]significance vs LC group

[c]significance vs LC + MgO/CS/Cis group

Effect of the MgO/CS/Cis on PTEN and mTOR Lung Proteins Levels by Western Immunoblotting Assay: The results demonstrated that the expressions of lung PTEN and mTOR were significantly downregulated in LC rats group, as compared to the corresponding normal control group. However, the data recognized ameliorations of these parameters in the lung of LC group treated with either Cis or MgO/CS/Cis as shown in (Table 3) and (Figure 5).

Table 3: Data expressed as mean ± standard error (mean ± SE), P value is significant at ≤ 0.05.

Group / Parameter	Control	Cis	MgO/CS/Cis	LC	LC+Cis	LC+MgO/CS/Cis
PTEN	$1.02^{b,c}$	$1.02^{b,c}$	$1.01^{b,c}$	$0.44\pm 0.01^{a,c}$	$0.81^{a,b,c}$	$0.77^{a,b}$
mTOR	$1^{b,c}$	$1.03^{b,c}$	$1.01^{b,c}$	$0.25^{a,c}$	$0.8^{a,b,c}$	$0.66^{a,b}$

Note: Data expressed as mean ± standard error (mean ± SE), P value is significant at ≤ 0.05.

[a]significance vs control group

[b]significance vs LC group

[c]significance vs LC + MgO/CS/Cis group

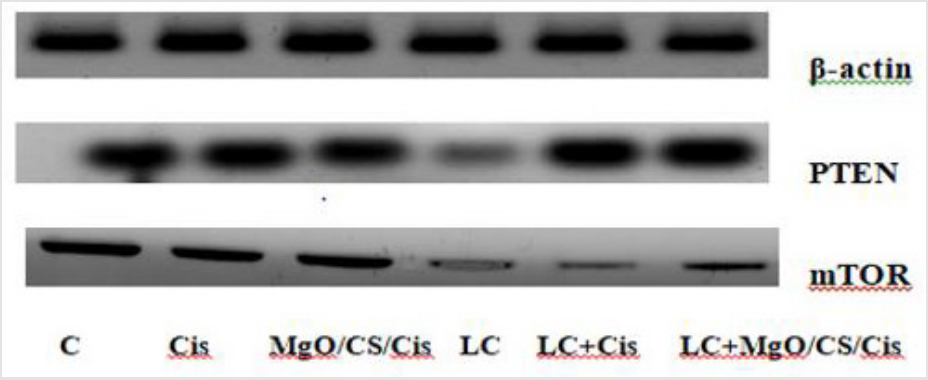

Figure 5: Immunoblotting analysis of phosphatase and tensin homolog (PTEN) and mechanistic target of rapamycin (mTOR) proteins. β -Actin was the loading control. Protein expression was detected by Western blot analysis.

AKT, PI3K and CAS-9 Lung Proteins Expression Levels: The data represented in (Table 4) showed that levels of both PI3K and AKT were significantly increased in rats with lung cancer when compared to control group but by treating with either Cis or MgO/CS/Cis the levels were significantly decreased. Also, expression level of CAS-9 decreased significantly in rats injected with urethane while increased significantly by treating with cis-pt and more decline in MgO/CS/Cis group as compared to LC group.

Table 4: Levels of AKT, PI3K and CAS-9 proteins expression levels in different groups.

Group / Parameter	Control	Cis	MgO/CS/Cis	LC	LC+Cis	LC+MgO/CS/Cis
AKT	$3.55\pm0.06^{b,c}$	$4.12\pm0.01^{b,c}$	$4.07\pm0.05^{b,c}$	$11.95\pm0.21^{a,c}$	$6.45\pm0.04^{a,b,c}$	$5.58\pm 0.21^{a,b}$
CAS-9	$2.06^{b,c}$	$1.8\pm0.01^{b,c}$	$1.81\pm 0.1^{b,c}$	$0.49\pm0.01^{a,c}$	$5.7\pm 0.15^{a,b,c}$	$4.7\pm 0.01^{a,b}$
PI3K	$2.4\pm0.05^{b,c}$	$2.97\pm0.0^{b,c}$	$2.39\pm0.05^{b,c}$	$9.8\pm 0.11^{a,c}$	$3.07\pm0.11^{a,b,c}$	$4.2\pm0.07^{a,b}$

Note: Data expressed as mean ± standard error (mean ± SE), P value is significant at ≤ 0.05.

[a]significance vs control group

[b]significance vs LC group

[c]significance vs LC + MgO/CS/Cis group

Histopathological Studies

The control groups exhibited the alveolar duct arises from respiratory bronchiole and numerous alveoli open into the alveolar duct. The oval alveoli lined by simple squamous epithelium and adjacent alveoli share a common inter-alveolar septum. The capillary plexuses are located in the thin septum, supported by fine connective tissue fibers, fibroblasts and other cells. At the free ends of the alveoli there are narrow bands of smooth muscle which is a continuation from the muscle layer of the respiratory bronchiole. The lung tissues showed necrosis without anaplastic cells, partial desquamation of bronchiolar epithelial with mild peri-bronchiolar around cell infiltrations which are detected with or without hemorrhage and lymphocytic pneumonia in Urethane + cis group (Figure 6). On the other hand, the alveolar tissues in LC + MgO/CS/Cis group showed normal lung consistencies without anaplastic cells or pneumonia. Some cases showed mild serofibrous deposit inside the alveoli or the lesions may be more aggressive into mild degenerative changes of inter-alveolar septa with an increasing of pneumocytes type-II and alveolar collapse.

Discussion

Nanoparticles because they are tiny and invasive, invade cancer cells and fight cancer effectively [18]. Magnesium oxide nanoparticles coated with chitosan nanoparticles were prepared using an improved chemical precipitation method which was used to encapsulate cisplatin to prepare MgO/CS/Cis nanocomposite. The consequences indicate that the copolymer chains effectively encapsulated the MgO/CS/Cis nanoparticles. Particles were used for cisplatin encapsulation and could be used in drugs distribution under moderate conditions. Our data findings provide promising drug-polymer nanocomposite for a controlled release drug system plan which enhanced tumor tissue permeability and retention effect for nanocomposite drug used. The present study demonstrates that cisplatin encapsulated MgO nanoparticles coated with chitosan have strong anti-growth properties and higher than cispaltin alone in a lung cancer. A549 cell line signified that MgO/CS / Cis NPs delivery systems can enhance the cytotoxicity *in vitro*.

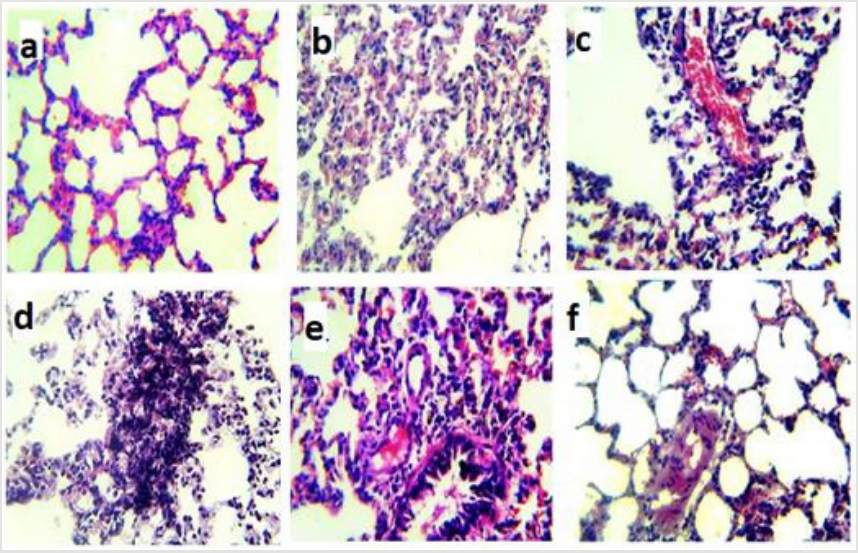

Figure 6: Microphotographs of histopathological examination of randomly selected lung sections of rats stained with hematoxylin and eosin and examined with a light microscope at 400× magnification.

(a) Lung from the Normal control group and

(b) MgO/CS/Cis treated group show the normal histological structure of alveoli.

(c) Lung from rats treated with (c) cisplatin group shows congested blood vessels, collapse of some alveoli with mild alveolar leukocytes infiltrations.

(d) Lung from rat treated with urethane (d) shows anaplastic changes of nucleus of pneumocytes type II in inter alveolar septa.

(e) Lung from (e) lung cancer induced rats treated with cisplatin shows peri-bronchiolar lymphocytic infiltration replaced lung alveoli.

(f) Lung from (f) lung cancer induced rat treated with MgO/CS/Cis shows mild serofibronous deposit inside some alveoli.

The MgO / CS / Cis nanoparticles could also become an effective chemotherapy tool for patients and could be ideal candidates for the production of drugs in these nanoparticles. It exhibited an excellent biocompatibility profile indicating its suitability for cancer targeting. It can accumulate at the tumor cells and increase tumor-based enhanced permeability and retention focusing and consequently reduce the drug dose required to achieve a higher anti-tumor effect and minimize toxicity. Besides, Chitosan is a hydrophilic polymer, which is why chitosan nanocomposites can become more extravassing and passive to prolong circulation of the blood [19]. PI3K/AKT/mTOR pathway is an intracellular signaling pathway which is vital for angiogenesis, cell proliferation, division, and survival [20]. Therefore, inhibition of the PI3K/Akt/mTOR pathway is predicted to exert antitumor action in lung cancer [21]. Actually, our results agree that inhibition of Akt and mTOR by MgO/CS/Cis NPs disallowed mTOR-prompted Akt stimulation and induced arresting antiproliferative effect by up-regulating PTEN.

In this study, rat model of lung cancer showed a significant induction for PI3K/AKT/mTOR pathway while marked suppression was detected in treatment with Cis which agrees with previous studies [22,23]. Additional, therapy with encapsulate MgO/CS/Cis NPs had a more suppressive effect on this pathway when compared with Cis only. Hindering of PI3K/AKT signaling pathway participated in sensitizing the resistant NSCLC cells to Cis after co-treatment with Wortmannin [24]. Previous study revealed that regulation of this signaling pathway was implicated in nanoparticles-mediated increase in the sensitivity of human pancreatic cancer cells to Cis therapy [25]. Also, gold nanoparticles treatment was documented to boost the sensitivity of colorectal cancer cells to cisplatin treatment via repressing PI3K/Akt signaling pathway in a concentration and time-dependent manner [26]. It has been reported that PTEN negatively controls the signalling pathway of PI3K / AKT, resulting in significantly reduced p-AKT, which controls the proliferation of the cancer cells [27]. Chitosan can more easily permeate the tumor cell membrane with a negative charge to ensure greater bioavailability in tumor cells [19].

Tumors initially respond to cisplatin, as damage, cell cycle arrests and death that decrease the tumor burdens significantly [28]. To clarify whether the up-regulation of PTEN by Cis and MgO/CS/Cis NPs led to the apoptosis of rats with lung cancer via mitochondrial pathway, we detected the levels of Bcl-2, caspase-9. Our result provides genetic evidence that cisplatin efficacy depends on Bcl2 loss and caspase 9 induction. Caspase-9 acts as a key in the intrinsic or mitochondrial pathway which is involved in an important role in programmed cell death. Caspase-9 is started on the apoptosome multifaceted to continue catalytic status [29]. In

addition, ability of a cell to undergo mitochondrial apoptosis is governed by pro- and anti-apoptotic members of the BCL-2 protein family. The equilibrium of pro- versus anti-apoptotic BCL-2 proteins confirms fitting regulation of programmed cell death during progress and preserves organismal health. When unbalanced, the BCL-2 family can act as a barrier to apoptosis and facilitates tumor development and resistance to cancer therapy [30].

In our study, we first proved that MgO/CS/Cis NPs could intensificate the activation of caspase-9 through the inhibition of the PI3K/Akt/ mTOR signaling pathway and deactivating Bcl2 release, confirming that MgO/CS/Cis NPs prevents the resistance of cisplatin alone which linked to caspase-dependent apoptosis and PI3K/Akt/ mTOR pathway. Furthermore, components of RAS/RAF/ERK pathway have been involved in cellular proliferation, migration, invasion and differentiation. Dysregulation of this pathway was reported in numerous cancer types as melanoma, and leukemia as well as colon, lung, pancreatic, and ovarian cancers [31]. Our results revealed prominent elevations in gene expression of KRAS in lung cancer group and this is in accordance with the results obtained by Zheng, et al. [32]. Earlier investigations clarified that inhibition of RAS/RAF/MEK gesturing pathways resulted in obvious decreased in proliferation, invasion and migration in NSCLC cells [33].

Administration of Cis or MgO/CS/Cis NPs in our study resulted in a reduction in KRAS mRNA level in comparison with LC group indicating that repressing of KRAS pathway was involved in the antineoplastic action of both therapeutic agents and this agrees with former results [34]. The group exposed to MgO/CS/Cis NPs achieved strong inhibition of this pathway. Use of Chitosan in our newly synthesized Cis nanocomposite which can exhibit anticancer activity is related to its ability in tumor cell biodistribution and drug accumulation. Adhikari and Yadav, et al. [1]. concluded pharmacokinetic *in vivo* study which revealed that mifepristone loaded chitosan nanoparticles confirm controlled drug delivery in a continued release manner and improve the oral bioavailability and drug antitumor action.

Conclusion

In summary, from the aforementioned results, it can be concluded that the newly synthesized Cis nanocomposite (MgO/CS/Cis NPs) resulted in no toxicity toward normal animals. Furthermore, our results provide strong molecular evidence in support of our hypothesis that synthesized Cis nanocomposite (MgO/CS/Cis NPs) augments cisplatin-induced anti-tumor effects on lung cancer rat model via inhibiting PI3K/AKT signal pathway, activating mitochondrial pathway, and down-regulating gene expression of K-RAS mRNA by up-regulating PTEN both *in vitro* and *in vivo*. These findings were well appreciated with histopathological studies suggesting that cis-platin nanocomposite can serve as a good therapeutic agent for the treatment of lung carcinoma with low toxicity side effects which should attract further studies.

Acknowledgement

My profound thanks to Dr. Ahmed Amer El-kady, associated professor of histopathology, national center for radiation research and technology, Egyptian Atomic energy authority, for his assistance in histopathology investigation.

Author's Contributions

Faten I. Abou El Fadl and Fatma S.M. Moawed: Conceptualization, Methodology, and Software Aya Sh.R. Shaaban: Data curation, Writing- Original draft preparation. Marwa G.A. Hegazy: Visualization, Investigation and Writing. Ahmed M.H. Salem: Supervision and Writing: Ekrami A. Hassan and Faten I. Abou El fadl: Software, Validation: Fatma S.M. Moawed: Writing- Reviewing and Editing.

Declaration of Conflicting Interests

The author(s) declared no potential conflicts of interest with respect to the research, authorship, and/or publication of this article.

Funding

The author(s) received no financial support for the research, authorship, and/or publication of this article.

Ethical approval: Not applicable.

Consent to Participate

Not applicable.

Consent to Publish

Not applicable. All authors approved for publication.

Data Availability Statement

The data that support the findings of this study are available from the corresponding author upon reasonable request.

References

1. Bray F, Ferlay J, Soerjomataram I, Siegel RL, Torre LA, et al. (2018) Global cancer statistics 2018: GLOBOCAN estimates of incidence and mortality worldwide for 36 cancers in 185 countries. CA Cancer J Clin 68(6): 394-424.
2. Mahboub BH, Vats MG, Zaabi A Al, Iqbal MN, Safwat T, et al. (2017) Joint statement for the diagnosis, management, and prevention of chronic obstructive pulmonary disease for Gulf Cooperation Council countries and middle East-North Africa region. Int J COPD 12: 2869-2890.
3. Koyi H, Johansson L, From J, Nyrén S (2015) Biopsy testing in an inoperable, non-small cell lung cancer population-A retrospective, real-life study in Sweden. J Thorac Dis 7(12): 2226-2233.

4. Hassan Lemjabbar Alaouia OH, Yanga YW, Buchanana P (2017) Lung cancer: biology and treatment options. Physiol Behav 176(5): 139-148.
5. Dasari S, Bernard Tchounwou P (2014) Cisplatin in cancer therapy: Molecular mechanisms of action. Vol. 740, European Journal of Pharmacology. Elsevier 740: 364-378.
6. Rosenberg B, VanCamp L (1970) The Successful Regression of Large Solid Sarcoma 180 Tumors by Platinum Compounds. Cancer Res 30(6): 1799-1802.
7. Florea AM, Büsselberg D (2011) Cisplatin as an anti-tumor drug: Cellular mechanisms of activity, drug resistance and induced side effects. Cancers (Basel) 3(1): 1351-1371.
8. Baetke SC, Lammers T, Kiessling F (2015) Applications of nanoparticles for diagnosis and therapy of cancer. Br J Radiol 88(1054): 20150207.
9. Jabir NR, Tabrez S, Ashraf GM, Shakil S, Damanhouri GA, et al. (2012) Nanotechnology-based approaches in anticancer research. Int J Nanomedicine 7: 4391-4408.
10. Choi YE, Kwak JW, Park JW (2010) Nanotechnology for early cancer detection. Sensors 10(1): 428-455.
11. De Jong WH, Borm PJA (2008) Drug delivery and nanoparticles: Applications and hazards. Int J Nanomedicine 3(2): 133-149.
12. Gomha SM, Edrees MM, Altalbawy FMA (2016) Synthesis and characterization of some new bis-pyrazolyl-thiazoles incorporating the thiophene moiety as potent anti-tumor agents. Int J Mol Sci 17(9): 1-11.
13. Gomha SM, Salaheldin TA, Hassaneen HME, Abdel Aziz HM, Khedr MA (2016) Synthesis, characterization and molecular docking of novel bioactive thiazolyl-thiazole derivatives as promising cytotoxic antitumor drug. Molecules 21(1): 1-17.
14. Parashar P, Rathor M, Dwivedi M, Saraf SA (2018) Hyaluronic acid decorated naringenin nanoparticles: Appraisal of chemopreventive and curative potential for lung cancer. Pharmaceutics 10(1): 33.
15. Emami Bistgani Z, Siadat SA, Bakhshandeh A, Ghasemi Pirbalouti A, Hashemi M (2017) Interactive effects of drought stress and chitosan application on physiological characteristics and essential oil yield of Thymus daenensis Celak. Crop J 5(5): 407-415.
16. Balamurugan S, Ashna L, Parthiban P (2014) Synthesis of nanocrystalline MgO particles by combustion followed by annealing method using hexamine as a fuel. J Nanotechnol 2014: 10-12.
17. Abdel Ghaffar AM, Abou El Fadl FI, El Sawy NM (2020) Radiation synthesis of polyvinyl alcohol/acrylic acid/magnesium oxide composite hydrogel for removal of boron from its aqueous solution. J Thermoplast Compos Mater 26(10): 1332-1348.
18. Liu CG, Han YH, Kankala RK, Wang S Bin, Chen AZ (2020) Subcellular performance of nanoparticles in cancer therapy. Int J Nanomedicine 15: 675-704.
19. Adhikari HS (2018) Anticancer Activity of Chitosan, Chitosan Derivatives, and Their Mechanism of Action. International Journal of Biomaterials, p. 27-38.
20. Xu F, Na L, Li Y, Chen L (2020) Roles of the PI3K/AKT/mTOR signalling pathways in neurodegenerative diseases and tumours. Cell Biosci 10(1): 1-12.
21. Yip PY (2015) Phosphatidylinositol 3-kinase-AKT-mammalian target of rapamycin (PI3K-Akt-mTOR) signaling pathway in non-small cell lung cancer. Transl Lung Cancer Res 4(2): 165-176.
22. Zhou D, Liu W, Liang S, Sun B, Liu A, et al. (2018) Apoptin-derived peptide reverses cisplatin resistance in gastric cancer through the PI3K-AKT signaling pathway. Cancer Med 7(4): 1369-1383.
23. Lu R, Zhao G, Yang Y, Jiang Z, Cai J, et al. (2019) Inhibition of CD133 Overcomes Cisplatin Resistance Through Inhibiting PI3K/AKT/mTOR Signaling Pathway and Autophagy in CD133-Positive Gastric Cancer Cells. Technol Cancer Res Treat 18(150): 1-11.
24. Zhang Y, Bao C, Mu Q, Chen J, Wang J, et al. (2016) Reversal of cisplatin resistance by inhibiting PI3K/Akt signal pathway in human lung cancer cells. Neoplasma 63(3): 362-370.
25. Wei MY, Shi S, Liang C, Meng QC, Hua J, et al. (2019) The microbiota and microbiome in pancreatic cancer: More influential than expected. Mol Cancer 18(1): 1-15.
26. Zhao X, Pan J, Li W, Yang W, Qin L (2018) Gold nanoparticles enhance cisplatin delivery and potentiate chemotherapy by decompressing colorectal cancer vessels. Int J Nanomedicine 13: 6207-6221.
27. Georgescu MM (2010) Pten tumor suppressor network in PI3K-Akt pathway control. Genes and Cancer 1(12): 1170-1177.
28. Oliver TG, Mercer KL, Sayles LC, Burke JR, Mendus D, et al. (2010) Chronic cisplatin treatment promotes enhanced damage repair and tumor progression in a mouse model of lung cancer. Genes Dev 24(8): 837-852.
29. Li P, Zhou L, Zhao T, Liu X, Zhang P, et al. (2017) Caspase-9: Structure, mechanisms and clinical application. Oncotarget 8(14): 23996-24008.
30. Campbell KJ, Tait SWG (2018) Targeting BCL-2 regulated apoptosis in cancer. Open Biol 8(5): 1-11.
31. McCubrey JA, Steelman LS, Chappell WH, Abrams SL, Montalto G, et al. (2012) Mutations and deregulation of Ras/Raf/MEK/ERK and PI3K/PTEN/Akt/mtor cascades which alter therapy response. Oncotarget 3(9): 954-987.
32. Zheng G, Shen Z, Chen H, Liu J, Jiang K, et al. (2018) Corrigendum to 'Metapristone suppresses non-small cell lung cancer proliferation and metastasis via modulating RAS/RAF/MEK/MAPK signaling pathway' [Biomed. Pharmacother 90(2017): 437-445] (S0753332217311605) Biomed Pharmacother 98: 925-926.
33. Samatar AA, Poulikakos PI (2014) Targeting RAS-ERK signalling in cancer: Promises and challenges. Nat Rev Drug Discov 13(12): 928-942.
34. Saliani M, Jalal R, Ahmadian MR (2019) From basic research to new achievements in therapeutic strategies of KRAS-driven cancers. Cancer Biol Med 16(3): 435-461.

ISSN: 2574-1241

DOI: 10.26717/BJSTR.2021.37.005934

Faten I Abou Albada. Biomed J Sci & Tech Res

Submission Link: https://biomedres.us/submit-manuscript.php